Materials Science and Engineering C 30 (2010) 990–996

Contents lists available at ScienceDirect

Materials Science and Engineering C

journal homepage: www.elsevier.com/locate/msec

Magnetite nanoparticles with high heating efficiencies for application in the hyperthermia of cancer

Zhixia Li [a,*], Masakazu Kawashita [a], Norio Araki [b], Michihide Mitsumori [c], Masahiro Hiraoka [c], Masaaki Doi [d]

[a] Graduate School of Biomedical Engineering, Tohoku University, 6-6-11-1306-1, Aramaki-Aoba, Aoba-ku, Sendai 980-8579, Japan
[b] National Hospital Organization Kyoto Medical Center, Kyoto 612-8555, Japan
[c] Graduate School of Medicine, Kyoto University, Kyoto 606-8507, Japan
[d] Graduate School of Engineering, Tohoku University, Sendai 980-8579, Japan

ARTICLE INFO

Article history:
Received 29 November 2009
Received in revised form 8 April 2010
Accepted 28 April 2010
Available online 6 May 2010

Keywords:
Hyperthermia
Magnetite nanoparticle
Particle size
Heat efficiency
Hysteresis loss

ABSTRACT

Magnetic hyperthermia is a safe method for cancer therapy. A gap-type alternating current magnetic field (100 kHz, 100–300 Oe) is expected to be clinically applicable for magnetic hyperthermia. In this study, magnetite nanoparticles (MNPs) varying in size from 8 to 413 nm were synthesized using a chemical coprecipitation and an oxidation precipitation method to find the optimum particle size that shows a high heating efficiency in an applied magnetic field. The particles' *in vitro* heating efficiency in an agar phantom at an MNP concentration of 58 mg Fe/ml was measured in an applied magnetic field. In a magnetic field of 120 Oe, the temperature increase (ΔT) of the agar phantom within 30 s was 9.3 °C for MNPs with a size of 8 nm, but was less for the other samples, while in a magnetic field of 300 Oe, $\Delta T = 55$ °C for MNPs with a size of 24 nm, and $\Delta T = 25$ °C for MNPs with a size of 8 nm. The excellent heating efficiency of MNPs with a size of 24 nm in a magnetic field of 300 Oe may be due to a combination of the effects of both relaxation and hysteresis losses of the magnetic particles. It is believed that MNPs with a size of 8–24 nm will be useful for the *in situ* hyperthermia treatment of cancer.

1. Introduction

Magnetic hyperthermia has recently attracted significant attention as a safe method for cancer therapy. It can increase the temperature in tumors to 41–46 °C, thereby killing the tumor cells with minimum damage to normal tissue. This method involves the introduction of ferromagnetic or superparamagnetic particles into the tumor tissue, followed by irradiation using an alternating current (AC) magnetic field. In general, magnetic particles generate heat in an external AC magnetic field from several physical mechanisms. These include relaxation loss or hysteresis loss, which strongly depends on the frequency of the external field, as well as the nature of the particles, such as the particle size and surface modifications [1,2]. Ferromagnetic particles generate heat (P) due to hysteresis loss, which is described by Eq. (1) [3]:

$$P = f\Delta U, \tag{1}$$

where f is the frequency and ΔU is the area of the hysteresis loop in an applying field.

Superparamagnetic particles generate heat (P) due to the relaxation loss (either Néel or Brown relaxation), which is approximated by [4]:

$$P = \pi \mu_0 \chi f H^2, \tag{2}$$

where f, H, χ, and μ_0 are the frequency, the magnetic field strength, the imaginary part of the magnetic susceptibility, and the permeability of free space, respectively.

Modern studies on hyperthermia of cancer have focused on developing intracellular hyperthermia systems. In these studies, superparamagnetic magnetite nanoparticles (MNPs) (with a size around 10 nm) are usually modified using dextran or oleic acid, and are functionalized with a polymer or liposome, and/or are further conjugated with an anticancer therapeutic drug to attempt to improve the colloidal stability of the magnetic fluid, affinity for the carcinoma cell, or confer a tumor-specific targeting ability [5–8]. These modified magnetic particles show an improved adsorption and accumulation in the area of a tumor, and also have an improved heating efficiency on exposure to an AC magnetic field. As reported by Ito et al. however, a local injection of magnetite cationic liposome (MCL) into glioma of rat caused transient accumulation of MCL in spleen of rat by 4 days after injection [5,6]. Mitsumori et al. reported that dextran-modified magnetite magnetic fluid could escape into the systemic circulation and was easily decomposed into dextran and iron oxide by the reticuloendothelial system

* Corresponding author. Tel.: +81 22 795 3937; fax: +81 22 795 3937.
E-mail address: zhixia@ecei.tohoku.ac.jp (Z. Li).

0928-4931/$ – see front matter © 2010 Elsevier B.V. All rights reserved.
doi:10.1016/j.msec.2010.04.016

when it was used as thermoseed for cancer treatment. Therefore, we still have fears that magnetic particles used are very small (some dozens of nanometer) and hence they are easily carried away by blood flow and disperse to unexpected other organs or tissues after a short hyperthermia treatment [7,8].

Recently, ferromagnetic microspheres with a diameter = 20–30 μm have been proposed to be useful as thermo-seeds for inducing embolic hyperthermia in cancers, especially in tumors located deep inside the body [9]. These spheres can be entrapped in the capillary bed of the tumors when they are implanted into blood vessels near the tumors by a catheter. They can heat the cancers locally by their hysteresis loss when placed in an AC magnetic field. Also, the entrapment of the spheres in the capillary bed of the tumors can give therapeutic effects of embolization by the prevention of blood and nutrition supply to the tumors. A few groups have studied the heating properties of ferromagnetic particles in a low-frequency AC magnetic field (~100 kHz), which can allow for clinical hyperthermia [10–12]. Some of the results have shown that MNPs with a diameter of about 46 nm exhibit excellent heating efficiency because of their hysteresis loss in an AC magnetic field [12]. Therefore, microspheres containing MNPs with a high heating efficiency may be useful for the *in situ* hyperthermia treatment of cancer in an AC magnetic field.

Various types of equipment have been developed for generating AC magnetic fields for the hyperthermia of cancer. Solenoid-type equipment able to generate high frequencies is often used, but it has a limited working space [13–15]. High frequencies, such as those above 400 kHz, cause nonspecific heating due to eddy currents, and this restricts their clinical application [16]. In 2005, the first clinical application of magnetic fluid hyperthermia was carried out for treating prostate cancer. In this study, the feasibility of hyperthermia was evaluated using a magnetic fluid hyperthermia apparatus (MFH 300F, operating at 100 kHz with a variable field strength of 0–226 Oe) and aminosilane-coated Fe_3O_4 nanoparticles [17]. It was reported that the treatment was tolerated well without anesthesia using a specially designed cooling device. These results suggested that a frequency of 100 kHz was safe and practicable for medical use.

Our group has developed a gap-type apparatus for generating AC magnetic fields, which operates at a frequency of 100 kHz, with an adjustable field strength of 100–300 Oe and a treatment space of 10 to 250 mm [9]. It is expected that this apparatus will be used clinically, and will be able to induce heat in magnetic particles via hysteresis loss and/or relaxation loss. Superparamagnetic fluids [7,8] and ferromagnetic spheres [9] have also been used as thermo-seeds *in vitro* and *in vivo* heat studies in the apparatus developed. The main problem is still the low heating efficiency of the applied magnetic medium.

Many studies have shown that there is a size (d) dependence of the magnetic properties of a magnetic particle, with most empirical data showing that the coercive force (H_c) follows a $d^{-0.6}$ power law for large grain sizes, e.g., multidomain particles [18], and that H_c is proportional to d^6 for ultrafine particles [19]. Obviously, besides the physical properties of the magnetic media, the nature of the applied AC magnetic field is crucial for the effectiveness and reliability of tumor therapy. In this study, the size dependence of the heating efficiency of MNPs was studied in our gap-type AC field apparatus. A series of MNPs with different sizes were prepared in aqueous solution and their heating properties were measured in an applied magnetic field. We aimed to find the optimum particle size with a high heating efficiency in an applied magnetic field. The theoretical predictions and results of *in vitro* studies will be discussed later. It is expected that our findings will be useful for designing novel thermo-seeds for clinical hyperthermia using present-day magnetic field apparatus.

2. Materials and methods

2.1. Preparation of the MNPs

All the chemicals used in our experiments were of analytical reagent grade and were used without further purification. The sodium hydroxide (NaOH) (Wako Pure Chemical Industries, Osaka, Japan), iron (II) chloride ($FeCl_2$), and iron (III) chloride ($FeCl_3$) (Wako Pure Chemical Industries) used were dissolved in deionized and deoxygenated water. MNPs with different diameters were prepared using two chemical methods. To obtain smaller-sized MNPs, Sample A was prepared using a coprecipitation method. Although the stoichiometric ratio of Fe^{2+}/Fe^{3+} is 1:2 for the formation of Fe_3O_4 by using a coprecipitation method, we chose a slightly higher ratio of Fe^{2+} in this study, because Fe^{2+} is easily oxidized to Fe^{3+} in aqueous solution [20]. The detail of experiment was described as follows: 37.5 ml of a 0.1 M $FeCl_2$ aqueous solution was mixed with 50 ml of a 0.1 M $FeCl_3$ aqueous solution; the mixed liquid was then added to 935 ml of a 21 mM NaOH solution while stirring with pH change of NaOH solution from 13 to 9 by the addition of iron solution. This was followed by ultrasonic treatment for a period of 20 min, and finally, the solution was aged at 36.5 °C for a period of 8 h. The resultant precipitate was washed with pure water and ethanol and then dried at 60 °C for a period of 12 h under a nitrogen (N_2) atmosphere.

In addition, Samples B, C, D, E, and F were prepared using an oxidation precipitation method in a $FeCl_2$–$NaNO_3$–NaOH aqueous system in accordance with two procedures as described elsewhere [21]. Samples B and C were prepared as follows. Under a given molar ratio of $Fe^{2+}/NO_3^-/OH^- = 3:1:5$, a calculated amount of sodium nitrate ($NaNO_3$) was added into a predetermined volume of NaOH aqueous solution (0.1–0.5 M), which was sufficiently deaerated by N_2 gas. And then a predetermined volume of deaerated $FeCl_2$ aqueous solution (0.5 M) was added to the $NaNO_3$–NaOH solution under stirring at a rate of 400 rpm. After stirring for 15 min, the solution was subjected to ultrasonic treatment for 10 min and aged at 60 °C for 5 h. The precipitates were separated and washed with pure water and ethanol, and then dried at 60 °C for 24 h. On the other hand, Samples D, E and F were prepared as follows. Under a given molar ratio of $Fe^{2+}/NO_3^-/OH^- = 3:1:5$, a predetermined volume of $FeCl_2$ solution (0.1 or 0.5 M) was added slowly into NaOH solution (0.02 or 0.5 M) under stirring. After running out of the predetermined volume of $FeCl_2$ solution for 5 min, a calculated amount of $NaNO_3$ solution (0.5 M) was added slowly into the $FeCl_2$–NaOH solution and further stirred for 10 min, and then aged at 60 °C for 4 or 10 h.

2.2. Structural characterization

The crystalline phases of the materials were verified using powder X-ray diffraction (XRD, RINT-2200VL, Rigaku, Japan) using the following settings: X-ray source = Ni-filtered CuKα radiation; X-ray power = 40 kV, 40 mA; scanning rate = $2\theta = 2°$/min; and sampling angle = 0.02°. The particle size and crystal morphology of the samples were observed using a transmission electron microscope (TEM, HF2000, Hitachi, Japan). The particle size distributions of the samples were obtained statistically by measuring the size of 100 nanoparticles using the TEM images.

2.3. Magnetic properties of particles and magnetic hysteresis loss

The saturation magnetization (M_s) and coercive force (H_c) of the samples were measured using a vibrating sample magnetometer (VSM-5, Toei, Japan) in magnetic fields up to 10 kOe at room temperature at a frequency of 80 Hz. We assumed that the area of the hysteresis loop measured under the applied field (100 kHz, 300 Oe or 120 Oe) was the same as that measured in a field of 300 Oe or 120 Oe using the VSM. The heat generated by the samples was calculated using the following equation [10]:

$$P = f \oint HdB \times 10^{-7}, \tag{3}$$

where f and H are the frequency and the applied magnetic field, and B is the magnetization of the samples in the applied magnetic field. The

term $\oint HdB$ is the area of the hysteresis loop in the applied magnetic field. Therefore, in our calculations, $f = 100$ kHz and the area of hysteresis loop measured at 300 Oe or 120 Oe using the VSM was substituted for $\oint HdB$.

2.4. In vitro heating studies

The *in vitro* heat generated by the samples was measured as follows. The samples were separately dispersed in a hot agar solution (agar content = 1.1 wt.%) in a glass tube. This was followed by ultrasonic treatment for a period of 2 min, and the agar was then solidified in cold water. In this study, the concentration of the sample in the agar phantom was fixed at 58 mg Fe/ml, which was lower than that (86.9 mg Fe/ml) used in the first report on clinical trials of magnetite nanoparticles-mediated hyperthermia [17]. In accordance with a previous study [9], the glass tubes in which the samples were dispersed with the agar phantom were placed in an alternating magnetic field of 100 kHz, 120 Oe or 100 kHz, 300 Oe. The heat generated by the samples was investigated by measuring the change in temperature of the agar phantom as a function of time using a fluoroptic thermometer (Model-3000, Luxtron Corp., Santa Clara, CA, USA).

3. Results and discussion

3.1. Structure of the samples

Fig. 1 shows the XRD patterns of all the samples formed in solution by the coprecipitation and oxidation precipitation methods. The XRD patterns were similar, and consisted of sharp peaks near to 18.32, 30.10, 35.46, 43.08, 53.66, 57.07, and 62.64°, showing that all the synthesized nanoparticles could be identified as magnetite (Fe_3O_4) with an inverse spinel structure (ICDD = 19-0629 [22]). In addition, the lattice constant, a, calculated from the XRD patterns, was 0.8393 nm for Sample A, 0.8375 nm for Sample B, 0.8371 nm for Sample C, 0.8398 nm for Sample D, 0.8388 for Sample E, and 0.8384 nm for Sample F. When compared with the data of maghemite (γ-Fe_2O_3, 0.8345 nm), the lattice constants of all the samples were closer to the values of Fe_3O_4 (0.8396 nm) [23,24]. The change in lattice constant, a, may suggest the formation of intermediate ferrite particles with a composition between that of Fe_3O_4 and γ-Fe_2O_3.

Fig. 2 shows TEM photographs of all the samples. Samples A, B, and C contained nearly spherical particles (see Fig. 2A–C), Samples D and E were composed of cubic-shaped particles with a few spherical particles present (see Fig. 2D and E), and Sample F consisted mainly of hexahedral and octahedral particles (see Fig. 2F). Some relatively larger particles in Sample E exhibited a thin plate-like shape compared with Sample F. Fig. 2 also shows that agglomeration of the particles occurred in all the samples because of the magnetic interaction usually of a dipole nature between the nanoparticles.

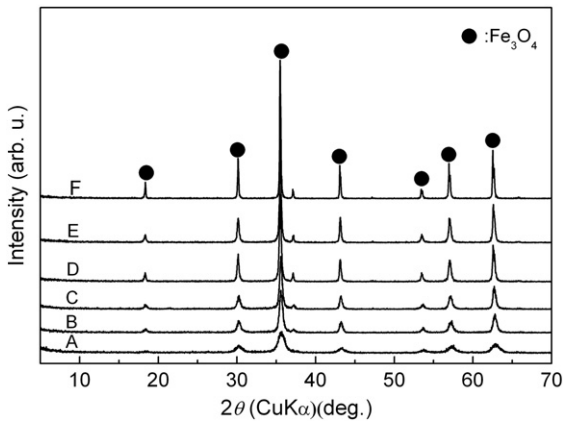

Fig. 1. XRD diffraction patterns of Samples A–F prepared by a coprecipitation method (A) and an oxidation precipitation methods (B–F).

Some literatures reported that γ-FeOOH or α-FeOOH phases were obtained in the precipitated nanoparticles when Fe_3O_4 was prepared at a temperature lower than 60 °C by a coprecipitation method [25]. This would be due to the presence of dissolved oxygen in reaction solution because the content of dissolved oxygen in aqueous solution is higher at a low temperature. Under the condition of absence of dissolved oxygen, it is believed that the temperature would affect mainly the particle size, and a high temperature would lead to the formation of nanoparticles with the larger particles size [26]. In the present study, we used the deoxygenated water to prepare the NaOH solution, therefore, only Fe_3O_4 and/or γ-Fe_2O_3 were precipitated even at a lower temperature than 60 °C. In fact, TEM observation showed that no rod-like α-FeOOH or vein-like γ-FeOOH crystal as described in literature [25], was formed in all samples.

Fig. 3 shows the particle size distribution of Samples A–F. The percentage ratio of the standard deviation to the mean size of the particle distribution are 18.8% for Sample A, 22.5% for Sample B, 25.6% for Sample C, 38.5% for Sample D, 35.3% for Sample E and 28.2% for Sample F. The wide size distribution in Samples D and E may be responsible for the obvious flocculation of the particles, because smaller particles tend to settle in the gaps between the larger particles, decreasing the specific surface area. This is a result of the basic tendency of primary particles to reduce the surface energy. Sample F showed large particles size (mean size = 415 nm) and a high standard deviation (std. dev. = 116 nm), but a relatively low percentage ratio of the standard deviation to the mean size of the particle (28.2%), suggesting its relatively uniform particle size distribution.

3.2. Magnetic properties of the samples

The saturation magnetization (M_s) and coercive force (H_c) of the samples are shown in Table 1. The smaller value of M_s for Samples A, B, and C is attributed to the disordered surface spins [27] and/or the partial existence of γ-Fe_2O_3 in these samples, because γ-Fe_2O_3 has a lower value of M_s (56 emu/g) than Fe_3O_4 (92 emu/g) [28]. In addition, one theoretical prediction [11] claims that H_c is proportional to d^{-1} for larger grain sizes, H_c is proportional to d^6 for ultrafine particles, and that the dividing line (the exchange length, d_{ex}) between the two cases is calculated to be 27 nm. The particles in Samples A were superparamagnetic, the value of H_c is near to zero. The particles in Sample B and C had a single domain [29,30], the value of H_c increased with increasing particle size. The particles in Samples D, E and F were inferred to contain a multidomain structure. In this case, pinning is one of the main sources of the H_c, and increasing the particle size would result in a loss of more pinning sites [11]. Thus, Sample F had a lower value of H_c than Sample E and D. There a deviation from the theoretical prediction ($d_{ex} = 27$ nm), Sample D (65 nm) showed the highest value of H_c, this is likely due to not only the particles size, but also the larger shape anisotropy corresponding to its cubic crystal structure (Fig. 2D).

Fig. 4 shows the magnetization (M) curves of Samples A–F under magnetic fields (H) up to 300 Oe at room temperature. We could estimate the magnetic loss caused by the hysteresis properties by integrating the area of the hysteresis loop according to Eq. (3), where $f = 100$ kHz and the maximum value of H is 300 Oe. The value of the hysteresis loss (P) was obtained, and is listed in Table 1. For Sample A, heat generated by the hysteresis loss was very small because of its superparamagnetic properties. When the particle size was greater than 24 nm, the hysteresis loop area decreased with increasing particle size. The dependence of loop area on particle size is similar to that of coercivity on particle size. The particle size of Sample B (24 nm) was nearest to the exchange length d_{ex} (27 nm) [12], the energy barrier of Sample B for reorientation of the magnetic moment was the highest,

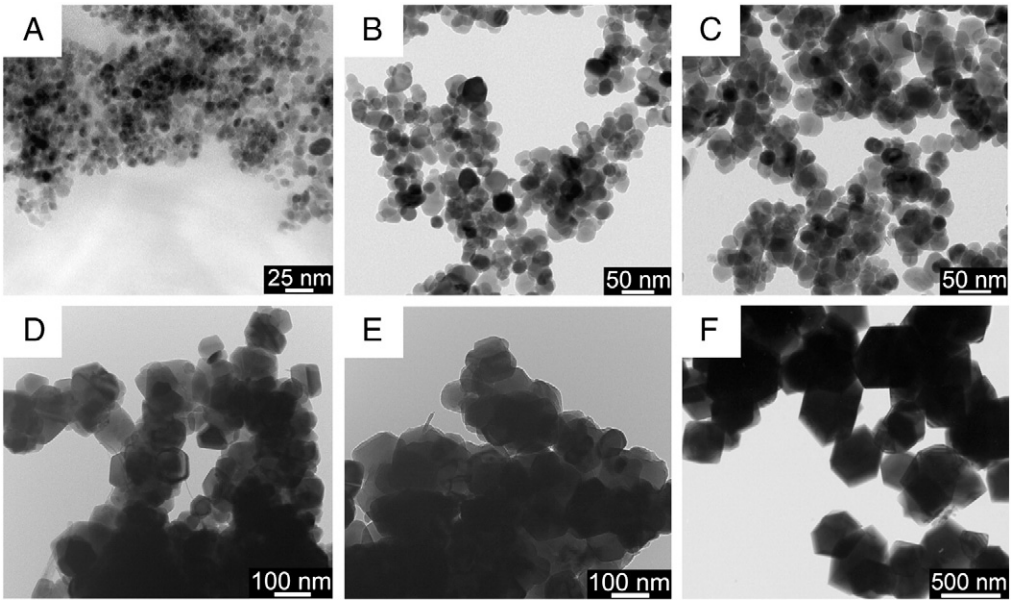

Fig. 2. TEM photographs of Samples A–F.

thus Sample B gave the largest hysteresis loop area. Samples D, E and F contained a multidomain structure, and the coercive force as well as the needed energy to continue domain wall motion decreased with increasing the particle size, thus they showed a decreased loop area. In addition, Samples C and D exhibited high H_cs under a saturated magnetic field (10 kOe), but their full hysteresis loop could not be obtained under a restricted field amplitude (300 Oe). Consequently, hysteresis loop areas of Samples B–F decreased with increasing particles size.

Fig. 5 shows the magnetization (M) curves of Samples A–F under magnetic fields (H) up to 120 Oe at room temperature. In this case, the loop areas for all samples were narrow, indicating that heat generations due to their hysteresis losses were very low. Our evaluation was a first-order approximation, since a hysteresis loop in an AC field should be different from a hysteresis loop measured in a static field.

3.3. In vitro heat generation of the samples

To avoid evaluation errors and to obtain the absolute heating results, the specific absorption rate (*SAR*) of each sample was analyzed using the data from the *in vitro* heat studies. Fig. 6 shows the time-dependent temperature curves of the agar phantoms in which the samples were dispersed in two different AC magnetic fields: (a) 300 Oe and (b) 120 Oe at 100 kHz. In the 300 Oe magnetic field, the temperature increase (ΔT) in the agar phantom within a period of

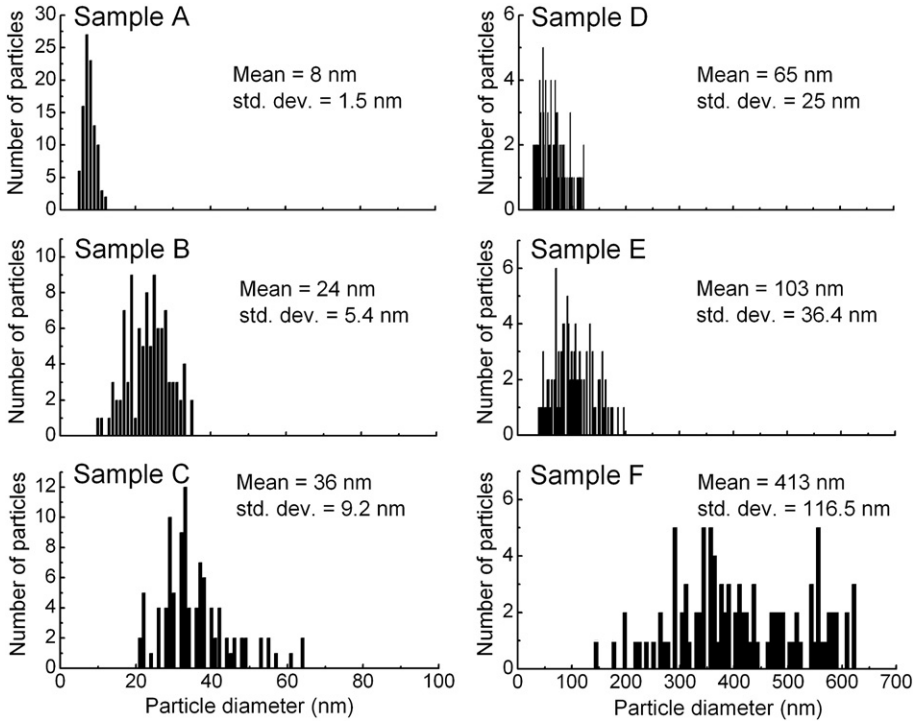

Fig. 3. Particle size and size distribution for Samples A–F.

Table 1
Particle sizes, magnetic properties and heating properties of samples.

Sample	Mean size (nm)	M_s (emu/g)	H_c (Oe)	P (W/[g of Fe])[a]	SAR (W/[g of Fe])[b]	SAR (W/[g of Fe])[c]
A	8	67.3	8.2	1.1	52.8	17.2
B	24	76.5	106.1	55.1	134.1	3.7
C	36	76.7	139.8	26.9	31.0	1.1
D	65	89.2	189.3	22.0	23.3	2.2
E	103	79.3	175.0	16.3	7.2	1.3
F	413	91.3	84.0	15.3	10.6	0.6

[a] Loss power per mass Fe estimated from 100 kHz and a loop area measured under magnetic field of up to 300 Oe at 80 Hz.
[b] Calculated from heating curve in agar phantom of per mass Fe measured under the applied magnetic field of up to 300 Oe at 100 kHz.
[c] Calculated from heating curve in agar phantom of per mass Fe measured under the applied magnetic field of up to 120 Oe at 100 kHz.

30 s was 55 °C for Sample B and 25 °C for Sample A, and decreased with increasing particle size (i.e., Sample B>Sample C>Sample D>Sample F). Sample B (24 nm in size) exhibited a high heating efficiency in the AC magnetic field. Comparing the data in Figs. 4 and 6, we can see that the particles with larger hysteresis loop areas also showed higher heating efficiencies in the applied magnetic field (300 Oe). In this case, the applied magnetic field strength was much higher than the value of H_c of all the samples, as listed in Table 1. Hence, the contribution to the generated heat due to the hysteresis losses was enhanced in these samples. Sample E exhibited a lower temperature increase than Sample F. This is most probably attributable to its lower value of M_s, as well as its large shape anisotropy corresponding to its thin plate-like crystal structure (Fig. 2E), although further investigation on this is needed.

From the increase in temperature, the value of *SAR* was calculated using the following equation [27]:

$$SAR = \frac{\sum_i C_i m_i}{m_{Fe}} \frac{\Delta T}{\Delta t}, \tag{4}$$

where $C_i m_i$ is the heat capacity of each component whose temperature will be increased in the applied AC field ($C_{agar} = 4.2$ J/g K, $C_{magnetite} = 0.937$ J/g K) [31]. The term $\Delta T/\Delta t$ is the initial gradient of the time-dependent temperature curve. The value of *SAR* calculated for all the samples is listed in Table 1. At 100 kHz and 300 Oe, the reason for the high value of *SAR* for Sample A (52.8 W/g) was the magnetic particles' Néel relaxation loss in the applied AC magnetic field because of its superparamagnetic properties, which could not be calculated from its hysteresis loop area, as shown in Fig. 4A. The value of *SAR* of Samples B, C, and D was higher than their hysteresis losses estimated from the loop area, suggesting that the actual loss in the AC magnetic field was higher than that calculated from the loop area measured in a static field. The value of H_c of a ferromagnetic particle usually increases with increasing field frequency according to the following equation [32]:

$$H_c / H_k = 1 - [(k_b T / K_u V) \ln(1/\tau_0 f)]^{1/2}, \tag{5}$$

where H_c is the coercive force, H_k is the anisotropic magnetic field, k_b is Boltzmann's constant, T is the temperature, K_u is the anisotropy constant, V is the particle volume, f is the frequency, and τ_0 is the time constant. This may be responsible for the increase in hysteresis loss in the AC magnetic field, since an increase in the value of H_c leads to an increase of the area of the hysteresis loop in an AC magnetic field.

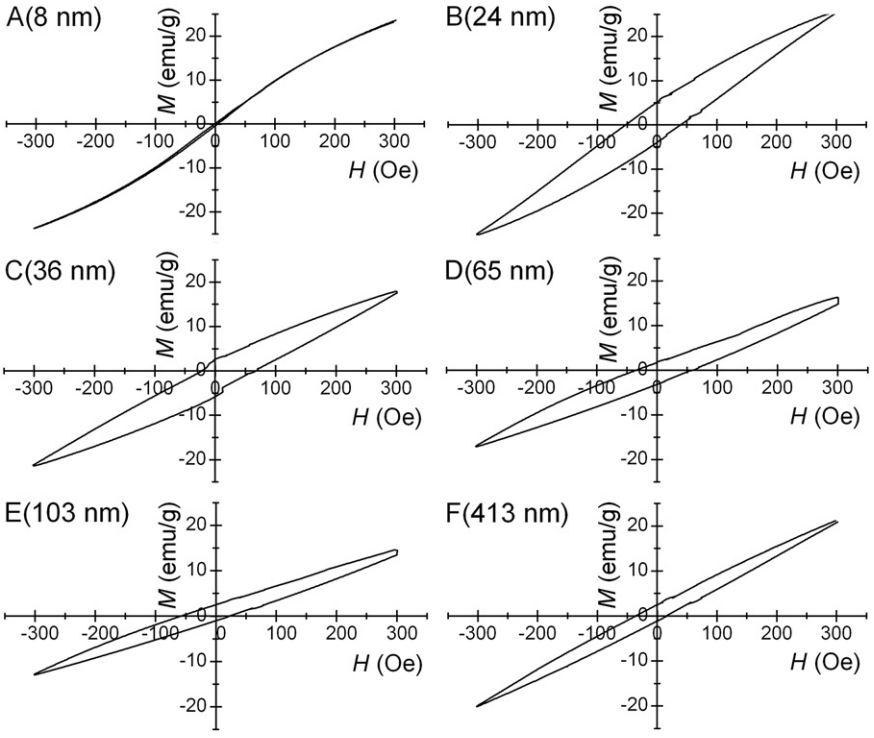

Fig. 4. Magnetization (M) curves of Samples A–F under magnetic fields (H) of up to 300 Oe at room temperature.

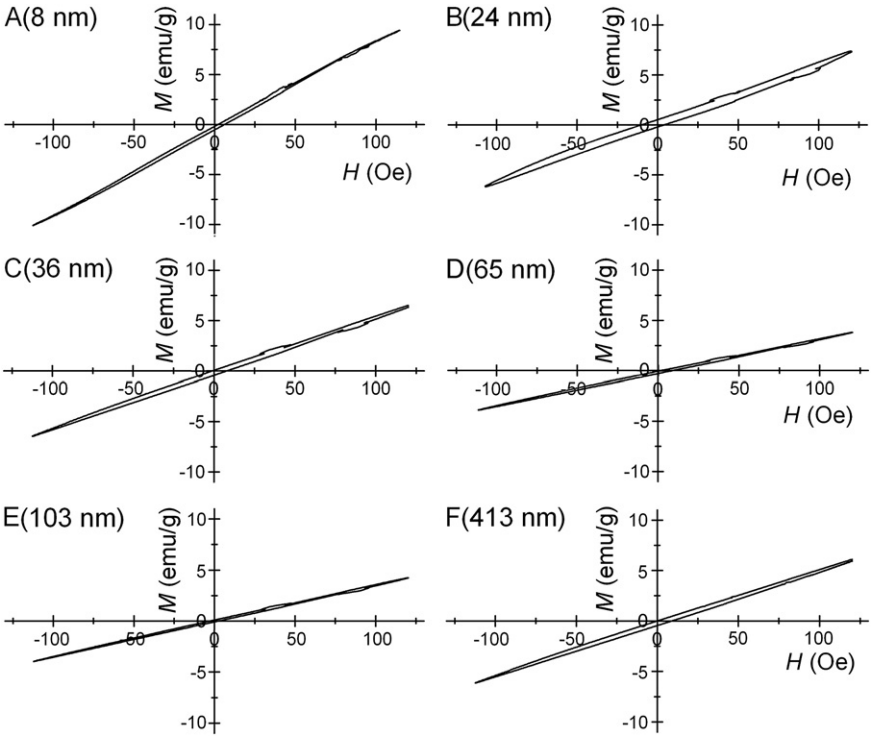

Fig. 5. Magnetization (M) curves of Samples A–F under magnetic fields (H) of up to 120 Oe at room temperature.

Similarly, the diameter of the MNPs, which can generate heat from hysteresis loss in an applied AC magnetic field, can be predicted by placing the value of H_c (the applied field strength = 100–300 Oe), $H_k = 400$ Oe, $K_u = 1.35$ kJ/m^3, $T = 298$ K, $f = 100$ kHz, and $\tau_0 = 10^{-9}$ s into Eq. (5). The obtained diameter of the MNPs was 44 nm at 300 Oe and 21 nm at 100 Oe. According to this prediction, the hysteresis loss will decrease or even reach zero when the particle size is greater than 44 nm in an applied field of 300 Oe, while in the case of an applied field of 100 Oe, the hysteresis loss will decrease for particle sizes greater than 21 nm. As can be seen in Table 1, the *in vitro* heating efficiency began to decrease from Sample C, which had a mean particle size of 36 nm. Therefore, as shown in Fig. 3, Sample C, which contained some particles greater than 44 nm, showed a slightly lower heating efficiency than Sample B (24 nm). In addition, the dependence of H_c to a high frequency was more pronounced for smaller ferromagnetic particles [33], which may be another reason for the high value of *SAR* for Sample B. Fig. 3 shows that Sample B also contained some superparamagnetic particles (<20 nm [33]); thus, the Néel relaxation loss contributed significantly to the heat generation in Sample B (heat generation due to Brownian relaxation was unavailable because Fe_3O_4

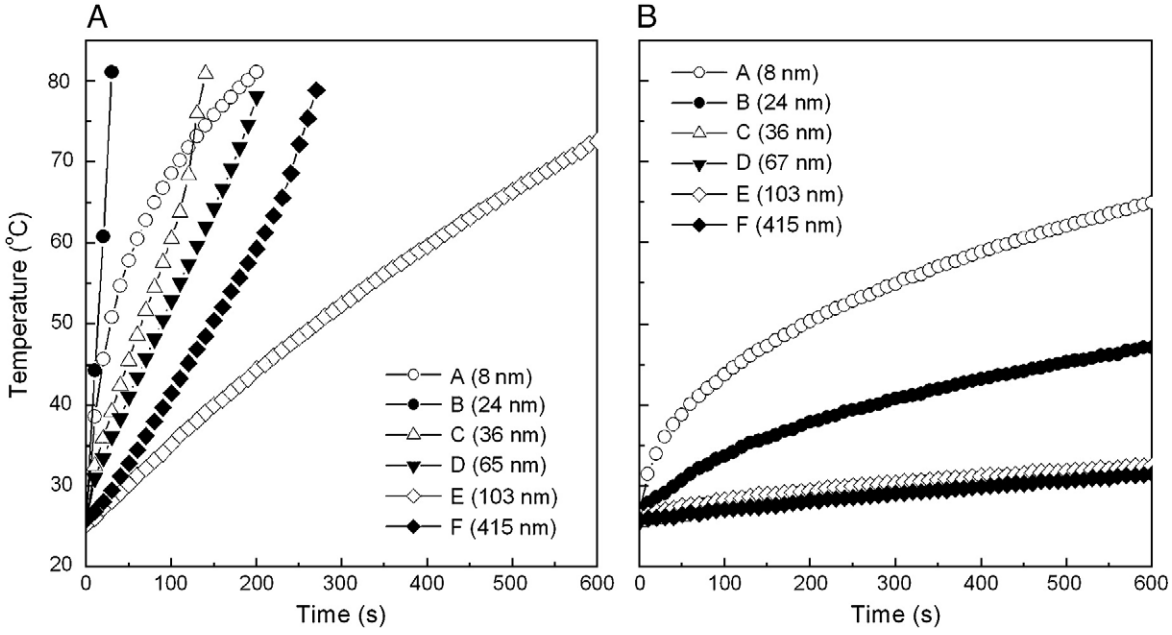

Fig. 6. Time-dependent temperature curves of the agar phantoms in which the samples were dispersed under two different AC magnetic fields: (A) 300 Oe and (B) 120 Oe at 100 kHz.

nanoparticles were fixed in agar medium). Samples D, E and F exhibited a lower heating efficiency which is most likely attributable to their multidomain structure.

In a field strength of 120 Oe, the temperature increase (ΔT) of the agar phantom within a period of 30 s was 9.3 °C for Sample A, 2 °C for Sample B, and 0.5–1 °C for the other samples. *SAR* values for all samples exposed to the AC field of 120 Oe have been calculated and shown in Table 1. Sample A showed a higher *SAR* value (15 W/g), and other samples showed a very low value. Particles in Sample A are superparamagnetic, therefore, heat generation is mainly due to its Néel relaxation loss and obviously decrease with decreasing magnetic field amplitude from 300 Oe to 120 Oe. The heat generated due to the hysteresis loss was low for Samples B–E, because the applied external magnetic field strength (120 Oe) was much lower than the value of H_c of these samples [34]. This can be referred from the small area of hysteresis loops measured under the magnetic field of 120 Oe by VSM (Fig. 5). This result can be predicted according to Eq. (5), where the allowed particle size is 22 nm, and so hysteresis loss will decreased rapidly when the particle size is greater than 22 nm. The heat generated in Sample B is significantly due to its Néel relaxation loss because of the presence of some superparamagnetic particles in the sample, as shown in Fig. 3B.

In general, hysteresis loop area demonstrates the heat generation due to hysteresis loss of sample under AC magnetic field. Heat generation due to relaxation loss cannot be estimated from loop area. In the case of 300 Oe, Sample A showed a smaller loop area but a higher value of *SAR* than those of Samples C–F, indicating Néel relaxation become an important contribution to *SAR* value of Sample A. The change in *SAR* values for Samples C–F with particle size showed a similar trend with that of hysteresis loop areas with particle size, suggesting that hysteresis loss is the main heating mechanism for these samples. For Sample B, whose *SAR* was much higher than that calculated from hysteresis loop area, suggesting that besides hysteresis loss, Néel relaxation contributed significantly the heat generation in Sample B. In the case of 120 Oe, the *SAR* values as well as hysteresis loop area of all sample decreased greatly, indicating that the magnetic field is too weak to continue domain wall motion for a larger particle (Samples D–F), and reorientating magnetic moment in single domain particle (Samples A–C) become difficult under the magnetic field of 120 Oe. The significant heat generated in Sample A is mainly due to its Néel relaxation loss.

It is ideal to evaluate the size-dependent heating properties of magnetic nanoparticles using particles having a narrow size distribution, but accurate classification of particle size is still difficult using present techniques, and therefore, we used the samples in their initial state (as-prepared) to clarify the main trends of the relationship between the heating properties and the particle size of the MNPs in an applied magnetic field. Based on our work, accurate classification of the particle size is the next step that can be performed selectively in a narrower particle size range.

There are several subjects that need further investigation prior to clinical application becoming possible.

(1) Our results show that superparamagnetic MNPs are useful in an applied field below 120 Oe, and MNPs with a size of 24 nm are useful in an applied field of 300 Oe. These data suggest that the optimal size of the MNPs that have high heating efficiency is present in the particle size range from 8 to 24 nm. Therefore, it is necessary to carry out further size clarification and characterization in this range. Further identification of the composition, perhaps using Mössbauer spectroscopy, is needed. The dependency relationship among particle size, field strength, and the heating properties of the particles needs to be clarified.
(2) Because of the high Curie point of the MNPs (580 °C), the temperature must be controlled by either adjusting the strength of the applied magnetic field or by controlling the concentration of the MNPs in the magnetic medium.

4. Conclusions

MNPs with a size around 8 nm exhibited a high heating efficiency in a magnetic field of 120 Oe, while MNPs with a size around 24 nm exhibited a high heating efficiency in high AC magnetic fields. The heating efficiency was the highest for MNPs with a size of 24 nm in 300 Oe magnetic fields at a frequency of 100 kHz, which may be because of the combined effect of the relaxation and hysteresis losses of the magnetic particles. The *SAR* values of samples with a single domain size were higher than those evaluated from the area of the hysteresis loop measured in a static field. It is believed that MNPs with a size around 8–24 nm will be useful for the *in situ* hyperthermia treatment of cancers in an AC magnetic field.

Acknowledgements

This work was partially supported by the Funds for Promoting Science and Technology under the Program for Exploring Advanced Interdisciplinary Frontiers, the Ministry of Education, Culture, Sports, Science and Technology, Japan, and research grants from the Kazuchika Okura Memorial Foundation, Japan.

References

[1] A. Jozefczak, A. Skumiel, J. Magn. Magn. Mater. 311 (2007) 193.
[2] M. Shinkai, M. Matsui, T. Kobayashi, Jpn. J. Hyperthermic Oncol. 10 (1994) 168.
[3] R. Hergt, W. Andrä, C.G. Ambly, I. Hilger, W.A. Kaiser, U. Richter, H.G. Schmidt, IEEE Trans. Magn. 34 (1998) 3745.
[4] R.E. Rosensweig, J. Magn. Magn. Mater. 252 (2002) 370.
[5] A. Ito, Y. Nakahara, K. Tanaka, Y. Kuga, H. Honda, T. Kobayashi, Jpn J. Hyperthermic Oncol. 19 (2003) 151.
[6] M. Yanase, N. Shinkai, H. Honda, T. Wakabayashi, J. Yoshida, T. Kobayashi, Jpn J. Cancer Res. 89 (1998) 463.
[7] M. Mitsumori, M. Hiraoka, T. Shibata, Y. Okuno, Y. Nagata, Y. Nishimura, M. Abe, M. Hasegawa, H. Nagae, Y. Ebisawa, Hepato-Gastroenterology 43 (1996) 1431.
[8] M. Mitsumori, T. Shibata, Y. Nagata, M. Hiraoka, M. Hasegawa, H. Nagae, K. Kito, Jpn. J. Hyperthermic Oncol. 17 (2001) 85.
[9] M. Kawashita, S. Domi, Y. Saito, M. Aoki, Y. Ebisawa, T. Kokubo, T. Saito, M. Takano, N. Araki, M. Hiraoka, J. Mater. Sci. Mater. Med. 19 (2008) 1897.
[10] A.A. Luderer, N.F. Borrelli, J.N. Panzarino, G.R. Mansfield, D.M. Hess, J.L. Brown, E.H. Barnett, Radiat. Res. 94 (1983) 190.
[11] N.F. Borrelli, A.A. Luderer, J.N. Panzarino, Phys. Med. Biol. 29 (1984) 487.
[12] M. Ma, Y. Wu, J. Zhou, Y. Sun, Y. Zhang, N. Gu, J. Magn. Magn. Mater. 268 (2004) 33.
[13] S. Wada, K. Tazawa, I. Furuta, H. Nagae, Oral Dis. 9 (2003) 218.
[14] N. Kawai, A. Ito, Y. Nakahara, H. Honda, T. Kobayashi, M. Futakuchi, T. Shirai, K. Tozawa, K. Kohri, Prostate 66 (2006) 718.
[15] K. Tazawa, S. Wada, M. Yatsuzuka, T. Saito, K. Tazawa, I. Nagano, K. Igarashi, I. Furuta, H. Nagae, Jpn. J. Hyperthermic Oncol. 19 (2003) 79.
[16] A. Ito, T. Kobayashi, Thermal Med. 24 (2008) 113.
[17] M. Johannsen, U. Gneveckow, L. Eckelt, A. Feussner, N. Waldöfner, R. Scholz, S. Deger, P. Wust, S.A. Loening, A. Jordan, Int. J. Hyperthermia 21 (2005) 637.
[18] F. Heider, D.J. Dunlop, N. Sugiura, Science 236 (1987) 1287.
[19] G. Herzer, J. Magn. Magn. Mater. 112 (1992) 258.
[20] K. Tao, H. Dou, K. Sun, Colloids Surf. A 320 (2008) 115.
[21] Z. Li, M. Kawashita, N. Araki, M. Mitsumori, M. Hiraoka, Trans. MRS-J. 34 (2009) 77.
[22] G.W. Leung, M.E. Vickers, R. Yu, M.G. Blamire, J. Cryst. Growth 310 (2008) 5282.
[23] T. Ozkaya, M.S. Toprak, A. Baykal, H. Kavas, Y. Koseoglu, B. Aktas, J. Alloy Compd. 472 (2009) 18.
[24] N. Mizutani, T. Iwasaki, S. Watano, T. Yanagida, H. Tanaka, T. Kawai, Bull. Mater. Sci. 31 (2008) 713.
[25] K.T. Wu, P.C. Kuo, Y.D. Yao, E.H. Tsai, IEEE Trans. Magn. 37 (2001) 2651.
[26] B. Tural, N. Özkan, M. Volkan, J. Phys. Chem. Solids 70 (2009) 860.
[27] L.Y. Zhang, H.C. Gu, X.M. Wang, J. Magn. Magn. Mater. 311 (2007) 228.
[28] B. Li, D. Jia, Y. Zhou, Q. Hu, W. Cai, J. Magn. Magn. Mater. 306 (2006) 223.
[29] V.S. Kalambur, B. Han, B.E. Hammer, T.W. Shield, J.C. Bischof, Nanotechnology 16 (2005) 1221.
[30] R.F. Butler, S.K. Banerjee, J. Geophys. Res. 80 (1975) 4049.
[31] S.A. Barringer, E.A. Davis, J. Gordon, K.G. Ayappa, H.T. Davis, J. Food Sci. 60 (1995) 1137.
[32] M.P. Sharrock, IEEE Trans. Magn. 26 (1990) 193.
[33] T. Atsumi, B. Jeyadevan, Y. Sato, K. Tohji, J. Magn. Soc. Jpn. 30 (2006) 555.
[34] R. Hergt, S. Dutz, R. Mueller, M. Zeisberger, J. Phys. Condens. Matter. 18 (2006) 2919.